

A Neural-Network-Based Mapping and Optimization Framework for High-Precision Coarse-Grained Simulation

Zhixuan Zhong^{1,2}, Lifeng Xu^{1,2}, Jian Jiang^{1,2*}

¹Beijing National Laboratory for Molecular Sciences, State Key Laboratory of Polymer Physics and Chemistry, Institute of Chemistry, Chinese Academy of Sciences, Beijing, 100190, P. R. China.

²University of Chinese Academy of Sciences, Beijing, 100049, P. R. China.

*Corresponding author(s). E-mail(s): jiangj@iccas.ac.cn;

Abstract

The accuracy and efficiency of a coarse-grained (CG) force field are pivotal for high-precision molecular simulations of large systems with complex molecules. We present an automated mapping and optimization framework for molecular simulation (AMOFMS), which is designed to streamline and improve the force field optimization process. It features a neural-network-based mapping function, DSGPM-TP (Deep Supervised Graph Partitioning Model with Type Prediction). This model can accurately and efficiently convert atomistic structures to CG mappings, reducing the need for manual intervention. By integrating bottom-up and top-down methodologies, AMOFMS allows users to freely combine these approaches or use them independently as optimization targets. Moreover, users can select and combine different optimizers to meet their specific mission. With its parallel optimizer, AMOFMS significantly accelerates the optimization process, reducing the time required to achieve optimal results. Successful applications of AMOFMS include parameter optimizations for systems such as POPC and PEO, demonstrating its robustness and effectiveness. Overall, AMOFMS provides a general and flexible framework for the automated development of high-precision CG force fields.

Keywords: Coarse-Grained, Molecular Dynamics Simulation, Graph Neural Network, Parameter Optimization

Introduction

In molecular science, accurate molecular characterization and analysis are crucial for elucidating the mechanisms within complex systems across various fields, including material synthesis [1, 2, 3] and biological processes. [4, 5, 6] While experimental methods have their limitations in temporal and spatial resolution, coarse-grained molecular dynamics simulations (CGMD) is a powerful and efficient method, enabling extended investigations of the microscopic mechanisms of macroscopic systems. [7, 8] In addition, coarse-grained (CG) molecular modeling provides a promising approach to bridge the atomic scale to micro scale, particularly in addressing the inherent limitations of all-atom models such as high computational cost and limited time scale. This method simplify the molecular complexity while retaining essential interactions and dynamics crucial for understanding the physics behind phenomena such as the self-assembly behaviors of amphiphiles. [9, 10, 11]

Nevertheless, the accuracy of CGMD is critically dependent on the precise parameterization of the force field. [12, 13] Top-down and bottom-up approaches are the most common strategy for constructing or optimizing force field parameters. The top-down method focuses on fitting macroscopic properties, ensuring that the simulations align with observable phenomena at larger scales. [14] Conversely, the bottom-up approach is concerned with reproducing microscopic statistics to maintain fidelity to atomic-level interactions and dynamics. [15] Among the universal CG force fields, the MARTINI force field [16, 17] stands out due to its straightforward mapping scheme and effective partitioning of CG bead energies. These make it one of the most popular molecular force fields for CGMD, balancing simplicity with a robust capacity to model a wide range of molecular systems effectively. Despite its widespread use, achieving high accuracy and correctly reproducing microscopic physics across various systems remains a significant challenge for both MARTINI2 and MARTINI3 iterations. [15, 18, 19, 20] In contrast, more specialized methods like the multiscale coarse-graining (MS-CG) technique [21, 22, 23] adopt a bottom-up strategy, focusing on accurately reproducing local statistical correlations and atomic forces, thereby offering a more detailed and precise approach to parameterization that aligns closely with empirical data. Recently, deep learning offers an innovative and precise approach to develop bottom-up CG potentials, [24] e.g., the CGnets [25] and neural network potentials (NNPs) for proteins [26]. Notably, the precision of these bottom-up CG force fields such as MS-CG series and CGnets heavily depends on the quality and detail of fine-grained datasets, such as atomistic trajectories and ab initio force/energy information. Moreover, bottom-up modeling approximates coarse-graining, reproducing structures at specific states. However, this treatment often fails in transferability and representability across different states and thermodynamic properties. [27]

Additionally, the multiscale mapping process often requires meticulous manual intervention and expertise. Striking the right balance between atomic detail and computational efficiency without compromising the model’s accuracy is a significant challenge. [15, 28] The precise mapping of atomic features to CG beads and the accurate parameterization of the force field are crucial factors that impact the performance and reliability of CGMD simulations. In fact, there are several tools available for parameter optimization in CGMD. However, as shown in Table 1, the existing algorithms for coarse-grained force field parameter optimization do not support automated mapping or the functionality for user-defined optimization schemes. To address these challenges, we present an automated mapping and optimization

framework for molecular simulation (AMOFMS), a Python package, designed to streamline the mapping and parameterization of CG force fields. This framework employs a graph-based neural networks to automate the mapping of atomistic structures to their corresponding CG representations. Moreover, AMOFMS incorporates multiple parallel optimizers, enabling more efficient exploration of complex molecular systems.

Table 1: Comparison with current CG parameter optimization toolkit.

Toolkit	Year	Mapping	Top-down	Bottom-up	Optimization algorithm
VOTCA[29]	2009	user-defined	✗	✓	IBI, IMC, FM
MagiC[30]	2013	user-defined	✗	✓	IBI, IMC
CAROL[31]	2019	user-defined	✓	✗	Bayesian
SwarmCG[32, 33]	2020	user-defined	✓	✓	FST-PSO
coarsen[34]	2023	user-defined	✗	✓	Adaptive gradient descent
OpenMSCG[35]	2023	user-defined	✗	✓	IBI, FM, REM
CGCompiler[36]	2023	user-defined	✓	✓	mv-PSO
AMOFMS (ours)	2024	auto/user-defined	✓	✓	PSO, GA, Simplex, Bayesian

IBI: Iterative Boltzmann Inversion; IMC: Inverse Monte Carlo; FM: Force Matching; REM: Relative Entropy Minimization; PSO: Particle Swarm Optimization; GA: Genetic Algorithm.

Results

Coarse-graining mapping and parameter optimization are crucial components for obtaining accurate and reliable results in CGMD simulations. AMOFMS is a comprehensive Python package that tailored for highly efficient parameter optimization of CG force fields, allowing users to implement customized rules and algorithms based on their personalized demands. In the next section, we will delineate the workflow for parameter optimization using AMOFMS and elucidate the functions of its principal modules.

Workflow of Parameter Optimization

As illustrated in Fig. 1a, AMOFMS initiates its workflow by accepting either SMILES or regular structure files (PDB, MOL2 and etc.) as input. Through a CG mapping process, these inputs are then transformed into a topological object in CG system., which includes force field parameters. During this phase, users can employ the DSGPM-TP (Deep Supervised Graph Partitioning Model with Type Prediction Enhancement) algorithm, which based on the MARTINI mapping rules, or they can opt for a custom mapping definition to execute this process.

Subsequent to the CG mapping, AMOFMS computes the loss (L) of the objective function. The objective function is designed to quantify the loss associated with target properties, which may include top-down macroscopic properties such as density and surface tension, or

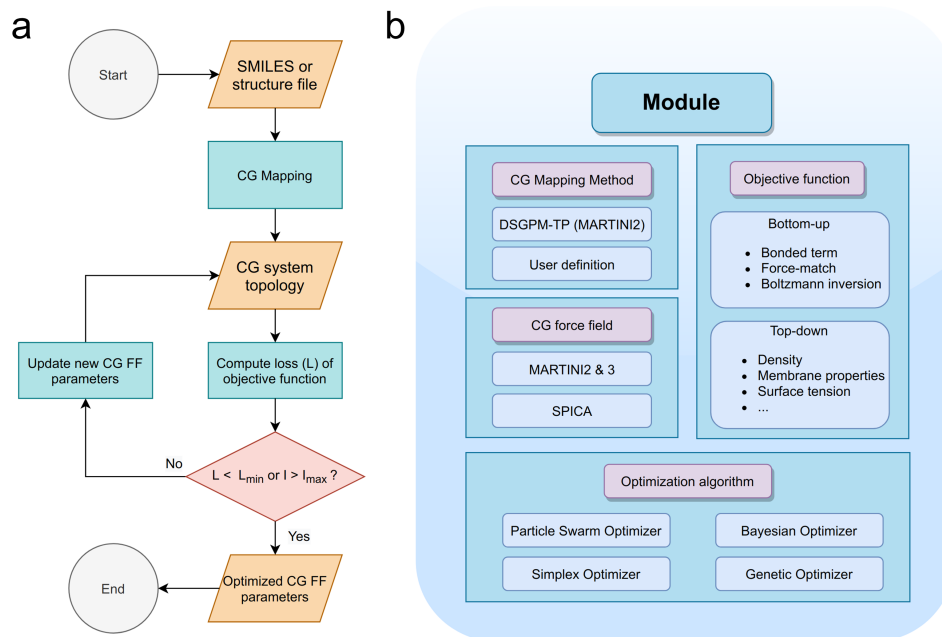


Fig. 1: (a) Workflow of CG force field parameter optimization using AMOFMS; (b) modules of AMOFMS.

bottom-up microscopic statistics like bond length and force, or potentially a combination of both.

Following the loss calculation, the optimizer evaluates whether the loss has reached a predefined minimum tolerance level (L_{\min}) or if the current iteration has reached the specified maximum limit (I_{\max}). If neither condition is met, the optimizer proceeds to update the CG force field parameters and repeats the cycle. This iterative process continues until the optimization criteria are satisfactorily met. Notably, our current AMFOMS exclusively supports parameter optimization for the MARTINI2,^[16] MARTINI3,^[17] and SPICA (SDK)^[37] force fields. Integration of user-defined potential functions is planned for future updates. The overall review of AMOFMS module is illustrated in Fig. 1b.

Mapping Methods

The process of coarse-grained mapping is an approach to reduce the number of degrees of freedom by grouping multiple atoms into larger units called “CG beads”. This reduction in complexity allows for more extensive and computationally feasible simulations. In general, selecting how atoms are grouped into beads relies heavily on the experts’ experiences and chemical and physical intuition.^[14] For instance, the popular MARTINI CG model typically groups four heavy atoms into a single CG bead.^[38] However, to improve the scalability and transferability of CG models, automating the mapping process is important. To address

this, motivated from DSGPM (Deep Supervised Graph Partitioning Model) [39], we propose a novel graph neural network framework named the DSGPM-TP (DSGPM with Type Prediction Enhancement), which can be used to automatically map atomistic structures to CG beads. This approach is aimed at replacing human experts’ intuition or experience. The DSGPM-TP formulates the prediction of CG mappings as a binary task that includes both a graph partitioning problem (atom clustering) and a multi-class classification task (atom-to-CG type prediction). This dual approach allows the model to first determine clusters of atoms that should be grouped together into beads (graph cut), and then categorize each cluster into specific types of CG beads based on their chemical and physical properties (multi-class classification).

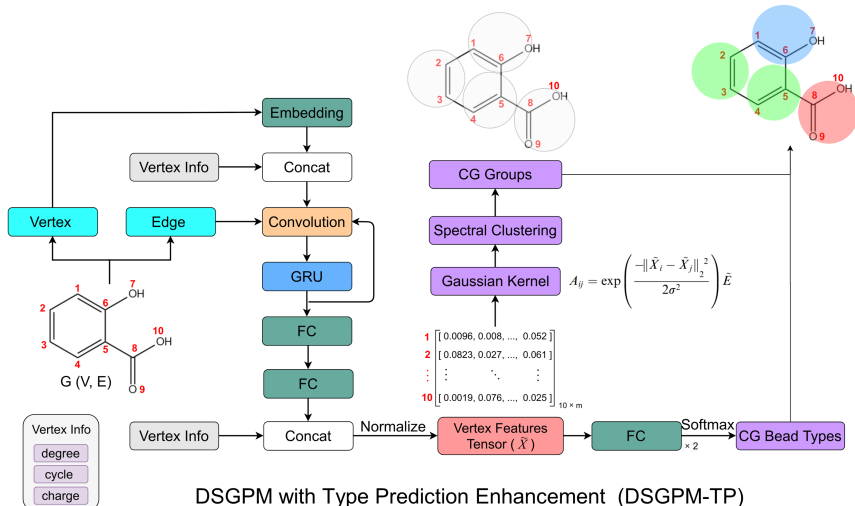


Fig. 2: Architecture of DSGPM-TP. FC denotes full-connected layer. Concat is concatenation. GRU refers to gated recurrent units.

As shown in Fig. 2, this architecture is designed to effectively generate robust atom features for spectral clustering and multi-class classification. It is based on the message passing neural network (MPNN) framework [40], enhancing its capability by concatenating specific atom metrics such as degree, charge, and cycle feat. This integration allows the model to capture the representative information of each atom, facilitating more accurate clustering and classification by providing comprehensive insights into the chemical environment and connectivity of the atoms. For the task of clustering atoms, as demonstrated in Table 2, our method surpasses existing state-of-the-art methods in terms of both AMI (Adjusted Mutual Information) [41] and graph cut metrics. This result confirms the effectiveness of our model in accurately capturing the essential features of molecular structures. Subsequently, the CG mapping results against ground-truth are visualized in Fig. 3 and S1. Overall, the DSGPM-TP shows good performance in CG mappings. Additionally, a series of ablation studies are conducted to examine the contributions of type loss, non-cut pair loss, vertex features,

and the number of fully-connected layers to the CG type prediction. The results, as shown in Table S1-S4, indicate the impact of each component on the overall performance of the DSGPM-TP model and their individual roles in enhancing prediction accuracy. Moreover, this comprehensive analysis validates the design choices made in developing DSGPM-TP.

While DSGPM-TP currently focuses on CG mappings based on MARTINI model, it can adapt to new consensus-based mappings in the future by training on updated datasets. This flexibility ensures DSGPM-TP remains a state-of-the-art tool for automating CG mapping.

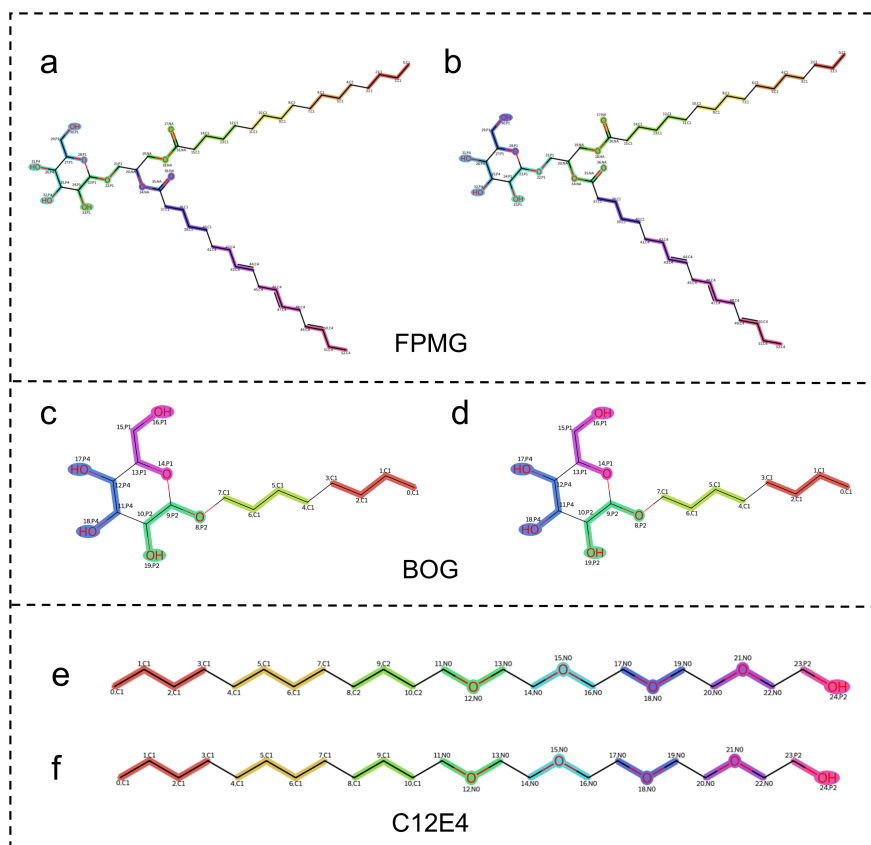


Fig. 3: Visualization of the CG mapping prediction and the ground truth. (a), (c), (e) are the ground truth. (b), (d), (f) are the results predicted by DSGPM-TP model. Atoms and their corresponding edges that belong to the same CG bead are highlighted with the same color. FPMG: C18:3/16:0 monogalactosyldiacylglycerol; BOG: 2-(hydroxymethyl)-6-octoxyoxane-3,4,5-triol; C12E4: tetraethylene glycol monododecyl ether.

Table 2: Comparison with state-of-the-art methods.

Method	AMI	Cut Prec.	Cut Recall	Cut F1-score
HDBSCAN [42]	0.5117	0.4631	0.4857	0.4205
FINCH [43]	0.6030	0.4602	0.8015	0.5595
h-NNE [44]	0.4230	0.3390	0.7637	0.4510
Gracius [45]	0.4205	0.2614	0.6826	0.3701
METIS [46]	0.7462	0.4968	0.5218	0.5038
Spectral Cluster [47]	0.8375	0.7000	0.6945	0.6971
DSGPM [39]	0.9139	0.8302	0.8314	0.8308
DSGPM-TP (ours)	0.9510	0.9029	0.9049	0.9038

Objective Functions

Parameter optimization is typically treated as a multi-objective optimization problem (MOP). This type of optimization involves managing several competing objectives that need to be simultaneously satisfied to achieve the most desirable overall outcome. A straightforward technique for implementing a MOP is scalarization, which involves converting the multiple objectives into a single objective. One common scalarization method is linear weighting, which is given by

$$Loss = \sum_i w_i f_i(\mathbf{x}), \quad (1)$$

where w_i represents the weight assigned to the i -th objective, f_i denotes the i -th objective function, and \mathbf{x} is the vector of parameters being optimized. The objective weights w_i play a crucial role in the optimization process as they help to balance the different parametrization targets. The setting of weight parameters is influenced by numerous factors, such as the specific molecular system, the requirements of the modeling task, and the quality of the training dataset. Using AMOFMS, users have the flexibility to configure multiple objective functions tailored specifically for the top-down process, the bottom-up process, or a combination of both.

Optimizer

In the AMOFMS, the optimizer module is responsible for calculating the objective functions corresponding to a given set of CG force field parameters and subsequently updating these parameters until the convergence criteria are met. Choosing an appropriate optimizer is a critical decision in the optimizing process, as it significantly impacts the efficiency and effectiveness of a optimization task. In the current version of AMOFMS, four optimizers are involved: Particle Swarm Optimizer (PSO), Bayesian Optimizer (BO), Genetic Optimizer (GO), and Simplex Optimizer (SO). These four optimization algorithms have been extensively employed across various fields, particularly in the development of force fields.[31, 36, 48, 49, 50] In our package, all optimizers utilize a parallel architecture to accelerate computational processes, and users have the flexibility to select either a single optimizer or a combination of multiple optimizers to effectively address the optimization task.

In the subsequent sections, we will illustrate the capabilities of AMOFMS through two practical examples, i.e., 1-palmitoyl-2-oleoylphosphatidylcholine (POPC) bilayer system with MARTINI2 Force Field and polyethylene oxide (PEO) system with MARTINI3 force field. Generally, we will outline the necessary steps to provide a concise overview of the workflow from initial setup to execution. The optimized parameters (denoted as Optimized CG) are then used in simulations and compared with the results from simulations based on the original force field parameters (denoted as Original CG) as well as experimental values to validate their accuracy and reliability. Each optimized and original system are carried out with three independent replicas, enabling us to ensure reproducibility and statistical reliability of the results.

Example 1: POPC with MARTINI2

POPC is a widely studied phospholipid that forms bilayer membranes, serving as model systems for biological membranes. The structural and dynamical properties of POPC membranes are crucial for understanding membrane behavior and interactions in biological systems. In this section, we demonstrate the optimization process of MARTINI2 CG force field parameters for the POPC membrane and present the results from the optimized model.

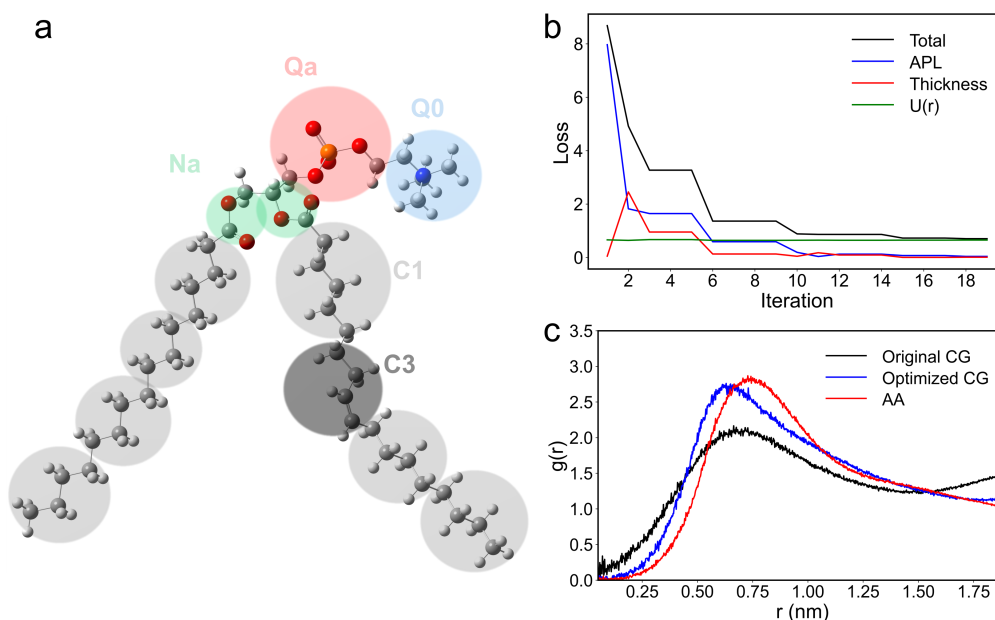


Fig. 4: (a) CG mapping of POPC predicted by DSGPM-TP model; (b) loss as a function of iterations; (c) radial distribution function between POPC molecules.

The CG mapping of the POPC molecule based on the DSGPM-TP model proposed in this work is illustrated in Fig. 4a. This mapping result aligns with the one recommended by the developers of the MARTINI force field, ensuring consistency and reliability in our

automated mapping model. The goal of this task is to fit both potential of mean force ($U(r)$) and macroscopic properties including the area per lipid (APL) and membrane thickness. The total loss (L) can be expressed as a weighted sum of deviations from target values for these properties:

$$L = L_{U(r)} + 10 \times (L_{\text{APL}} + L_{\text{thickness}}). \quad (2)$$

Subsequently, the PSO optimizer with 32 swarms and 20 iterations is employed to execute the optimization process. As shown in Fig. 4b, the total loss rapidly decreases with iterations. Table 3 compares the experimental values and those calculated by the original and optimized MARTINI2 models, demonstrating that the results from the optimized CG model aligns more closely with experimental data. Besides the APL and membrane thickness, the volume per lipid (VPL), isothermal area compressibility modulus (K_A), and the lateral diffusion coefficient (D_L) obtained from the optimized CG model also show good agreement with experiments, indicating that the optimizer not only accurately captures the structural properties of the POPC membrane but also reproduces other important properties such as the dynamic behavior (D_L). It is worth mentioning that, to avoid the effects of finite size, similar comparisons are conducted in larger boxes, as shown in Table S5. Furthermore, the employed bottom-up strategy ensures that the radial distribution function $g(r)$ between POPC molecules shows greater consistency with fine-grained models, such as the CHARMM all-atom force field (AA), as displayed in Fig. 4c. Moreover, bond and angle distributions obtained from the optimized CG model also show better agreement with the all-atom models (Fig. S2). These results demonstrates the capability of our AMOFMS to accurately develop coarse-grained models for complex biological systems.

Table 3: Properties of POPC membrane.

Method	Thickness (nm)	APL (nm ²)	VPL(nm ³)	D_L (*10 ⁻⁸ cm ² /s)	K_A (mN/m)
Original CG	4.019 ± 0.001	0.660 ± 0.000	1.372 ± 0.000	13.884 ± 0.365	306.612 ± 7.361
Optimized CG (ours)	3.724 ± 0.001	0.629 ± 0.002	1.203 ± 0.000	11.899 ± 0.360	309.980 ± 7.050
Experiment	3.70[51]	0.63[52]	1.223[53]	8.87-10.70 [54]	180-330 [55]

Example 2: PEO with MARTINI3

PEO is a polymer of significant interest in various fields such as materials science, biomedicine, and nanotechnology. Optimizing the force field parameters for PEO is crucial to ensure accurate predictions of the structural, thermodynamic, and dynamic properties of PEO systems. In this section, we outline the optimization process of the MARTINI3 CG force field parameters for PEO and discuss the results of the optimized model.

The PEO molecule is modeled based on the MARTINI3 representation, and the initial force field parameters are generated by the Polyply python software. [56] It is important to note that we use the TP1 bead to represent the termini of the polymer chain, rather than the SN3R bead recommended by Polyply, as shown in the Fig. 5a. This is because TP1 bead provides a more accurate polarity of the termini in the framework of the standard MARTINI3

representation. In this work, the system consists of 40 PEO chains with a polymerization degree of 52. The optimization process combines both bottom-up and top-down strategies. The bottom-up approach focuses on fitting the potential of mean force ($U(r)$) and CG forces, while the top-down approach targets macroscopic properties such as density and surface tension. This dual strategy ensures a comprehensive optimization that captures both micro- and macroscopic properties. The total loss is defined as

$$L = L_{U(r)} + L_{FM} + 10 \times L_{\text{density}} + 50 \times L_{\text{surface tension}}. \quad (3)$$

The Bayesian Optimizer is employed to perform the optimization. As shown in the Fig. 5b, this optimizer demonstrates a robust ability to reduce the loss function efficiently, achieving this with a lower computational cost (50 iterations with 200 initial samples).

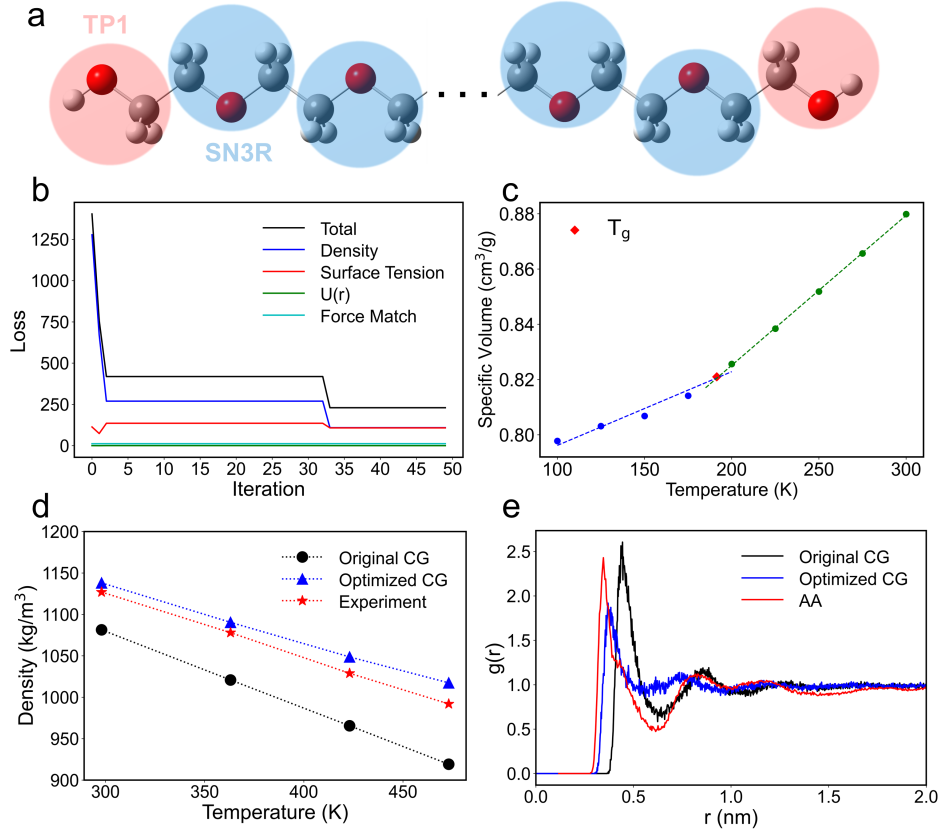


Fig. 5: (a) CG mapping of PEO; (b) loss as a function of iterations; (c) prediction of the glass transition points of PEO; (d) density of PEO system under different temperatures; (e) radial distribution function between TP1 beads.

Table 4: Properties of PEO system.

Method	Density (kg/m ³)	Surface Tension (mN/m)	T _g (K)
Original CG	1081.430 ± 0.014	31.887 ± 0.482	188.700
Optimized CG (ours)	1138.110 ± 0.093	40.077 ± 1.049	191.400
Experiment	1127 [57]	42.6 [57]	201.15 [58]

Although the original CG force field performed good, our AMOFMS-optimized CG force field shows even better agreement with experimental results, as shown in Table 4, where the glass transition temperature is identified by observing the slope of the curve of the temperature-dependent specific volume (Fig. 5c). Moreover, when applied to different temperatures, our CG force field predicts densities with errors within 1% compared to experiments (Fig. 5d), further demonstrating the success of AMOFMS. We have to note that, as shown in Table S6, the simulation results mentioned above are not affected by the size of the simulation box. Meanwhile, according to Fig. 5e and S3, our CG force field exhibits improved microscopic structure of PEO.

In summary, the successful applications of AMOFMS in both the POPC membrane and bulk PEO systems demonstrate its versatility and effectiveness. In fact, our AMOFMS can be utilized in a variety of systems to accurately study their microscopic and macroscopic properties.

Discussion

In this study, we have presented a comprehensive tool, AMOFMS (an Automated Mapping and Optimization Framework for Molecular Simulation), designed to streamline and enhance the development and optimization of coarse-grained (CG) force fields. AMOFMS addresses several critical challenges in the field of molecular simulations such as the automated CG mapping and flexible optimization framework, offering significant advancements over existing methodologies. Some of the key contributions of AMOFMS are listed as below:

1. Automated mapping functionality: One of the most notable features of AMOFMS is its automated mapping capability. This functionality simplifies the complex and labor-intensive process of CG mapping, thereby reducing human error and improving the reproducibility of molecular simulations.

2. Flexible optimization framework: AMOFMS allows users to define and customize a wide range of optimization parameters, e.g., Lennard-Jones potentials, bond lengths, force constants and so on. This flexibility enables the tool to be applied to a variety of molecular systems from simple systems with small organic molecules to complex systems with biomacromolecules.

3. Multi-objective optimization: AMOFMS supports multi-objective optimization by integrating both bottom-up (e.g., pair distribution function and force matching) and top-down (e.g., density and surface tension) approaches. This comprehensive framework ensures that the force fields trained by our AMOFMS can simultaneously account for both the microscopic and macroscopic properties of the system.

4. Parallel optimizer: The parallel optimizers greatly accelerate the optimization process, enabling AMOFMS to efficiently handle large and complex systems.

Despite its numerous advantages of AMOFMS, there are still some limitations that need to be addressed in future work:

1. Challenges in directly incorporating many-body interactions: Similar to most molecular force fields, AMOFMS considers intermolecular forces based on pairwise potential assumptions and does not directly account for many-body interactions. Accurately incorporating many-body interactions remains a significant challenge in molecular simulations.
2. Limit to specific force field models: In its current version, AMOFMS trains force fields using predefined models like the MARTINI models. This limitation may restrict its applicability to specialized molecular systems.
3. Underdeveloped gradient descent optimizer: The gradient descent optimizer has yet to be fully developed. However, deriving the analytical solutions for the differential forms of macroscopic properties with respect to force field parameters present significant challenges in our current version of AMOFMS. In fact, an automatic differentiation technique may offer a promising solution to this problem. One such example is DMFF, an open-source molecular force field development platform based on automatic differentiation.[\[59\]](#) We will consider automatic differentiation technique in our future work.

In conclusion, AMOFMS offers a robust, accurate, and efficient solution for development and optimization of force field. Its excellent features including automated mapping, flexible parameter selection, multi-objective optimization, and parallel optimizer collectively provide a powerful toolkit for force field development. Thus, it enables more accurate and efficient computational simulations, advancing our understanding of complex molecular systems. Furthermore, although the current version of AMOFMS is limited to specific force field models, its framework shows promising potential for the development and optimization of other fine- or coarse-grained force fields.

Methods

DSGPM-TP

Deep Supervised Graph Partitioning Model with Type Prediction Enhancement (DSGPM-TP) treats the CG mapping prediction as a graph partitioning problem. In this model, a molecule is represented as a graph $G = (V, E)$, where V consists of atom types encoded as one-hot vectors and E encodes bond types. One motivation for DSGPM-TP is to enhance spectral clustering, which heavily depends on the quality of an affinity matrix A . Spectral clustering performs well when the affinity matrix accurately represents the relationships between nodes. However, traditional methods often fall short by merely indicating the presence or absence of bonds but without capturing bond types or strengths. DSGPM-TP aims to create a refined affinity matrix that accurately distinguishes between different types of atomic interactions. Another motivation is to predict the type of the CG bead (cluster). This involves precisely identifying which atoms belong to the same CG bead type. This allows the model to provide insights into the global information of the molecule, which is crucial for practical applications across various fields such as molecular design.

Details of Model

Based on the MPNN framework, the graph neural network (GNN) extracts features for each atom, initially projecting one-hot encoded atom types into a higher-dimensional feature space through a multilayer perceptron (MLP). As shown in Fig. 2, this embedded feature is then enhanced with the atom’s degree (the number of chemical bond directly connected to the atom), charge, and a cycle indicator, resulting in a vertex feature tensor \tilde{X} . Specifically, the features generated by the GNN are updated using convolutional layers and gated recurrent units (GRU) to capture complex relationships between atoms. The feature matrix (X_0) is updated iteratively using the GRU layer over T time steps to produce the final feature matrix X_T .

$$\begin{aligned}\hat{X}_u^{t-1} &= \mathbf{W}' X_u^{t-1} + \sum_{v \in \mathcal{N}(u)} X_v^{t-1} \phi^e(E_{uv}), \\ X_i^t &= \text{GRU}(\hat{X}_u^{t-1}, H_u^{t-1}),\end{aligned}\tag{4}$$

where underscript u denotes u -th atom and superscript t denotes time step (layer); \mathbf{W}' is a weight matrix; superscript $'$ denotes transpose; the function $\phi^e(\cdot)$ is used to map the bond type E_{uv} to an edge-conditioned weight matrix, which is implemented as a MLP; and H_u^{t-1} is the hidden state of the GRU for atom u at the previous time step $t-1$. Subsequently, vertex features tensor \tilde{X} is obtained by:

$$\begin{aligned}\tilde{X}' &= \text{Concat}(\text{MLP}(X^T), V, I_{\text{degree}}, I_{\text{charge}}, I_{\text{cycle}}), \\ \tilde{X} &= \frac{\tilde{X}'}{\|\tilde{X}'\|_2},\end{aligned}\tag{5}$$

where I_{degree} , I_{charge} , and I_{cycle} represent degree, charge, and cycle indicator of each atom in a molecular graph, respectively. Here, the charge information is computed by Gasteiger-Marsili method implemented on RDKit.[60] Then, the affinity matrix A is computed using a Gaussian kernel, which measures the similarity between atom features:

$$A_{ij} = \exp\left(-\frac{\|\tilde{X}_i - \tilde{X}_j\|^2}{2\sigma^2}\right) \tilde{E},\tag{6}$$

where $\sigma = 1$ is the bandwidth. \tilde{E} represent the adjacency matrix:

$$\tilde{E}_{ij} = \begin{cases} 1, & \text{if atom } i \text{ and atom } j \text{ are bonded} \\ 0, & \text{otherwise} \end{cases}\tag{7}$$

Training

To train the model, the total loss (L) consist of graph cut loss (L_{cut}) and the type prediction loss (L_{type}):

$$L = L_{\text{cut}} + \lambda_1 L_{\text{type}}.\tag{8}$$

Graph cut loss is a type of loss function used in graph-based segmentation tasks. It measures the dissimilarity between regions in a graph that have been partitioned or segmented. Two

types of cut losses are used: cut triplet loss (L_{triplet}) and non-cut pair loss (L_{pair}). The cut triplet loss encourages the model to separate features of atoms in different partitions by a margin (α):

$$L_{\text{triplet}} = \frac{1}{|N_T|} \sum_{T_i=\{a,p,n\}} \max\left(\left\|\tilde{V}_a - \tilde{V}_p\right\|_2 - \left\|\tilde{V}_a - \tilde{V}_n\right\|_2 + \alpha, 0\right), \quad (9)$$

where $T_i = \{a, p, n\}$ denotes a specific triplet consisting of an anchor atom (a), a positive atom (p), and a negative atom (n). \tilde{V}_a , \tilde{V}_p , \tilde{V}_n are the feature vectors (embeddings) of the anchor, positive, and negative atoms, respectively. On the other hand, the non-cut pair loss unifies the features of atoms within the same partition.

$$L_{\text{pair}} = \frac{1}{|N_P|} \left\|\tilde{V}_a - \tilde{V}_{a'}\right\|_2. \quad (10)$$

The final graph cut loss is defined as

$$L_{\text{cut}} = L_{\text{triplet}} + \lambda_2 L_{\text{pair}}. \quad (11)$$

Type prediction loss is a loss function used to train models for predicting the type for the coarsed-grained group or cluster. The cross-entropy loss function is commonly used for this classification task, i.e.,

$$L_{\text{type}} = -\log\left(\frac{\exp(V_{\text{real}})}{\sum_j \exp(V_j)}\right). \quad (12)$$

The DSGPM-TP model is trained for 500 epochs, and the epoch that yields the best performance during the 5-fold cross-validation is selected. The hidden feature dimension is set to 128. The GNN implementation is built using PyTorch and PyTorch Geometric.[61, 62]

Dataset

The MARTINI2 dataset used to train and validate models in this work is collected from the published literature and MARTINI website (<http://md.chem.rug.nl/index.php/example-applications2>), encompassing a wide range of molecular structures and properties documented in scientific research. Each entry in the dataset comprises information regarding the molecular coarse-grained (CG) groups, e.g., the type of each group and the details about which atoms belong to this group. The current dataset consists of 744 entries.

MD settings and analysis of POPC Example

In this work, all the simulations (except for the analyses of surface tension) are performed in the isothermal-isobaric (NPT) ensemble using GROMACS 2021.4,[63] with periodic boundary conditions applied in all three spatial directions.

Details of fine-grained simulation

The initial POPC bilayer systems are constructed by CHARMM-GUI server.[64] Each system is composed of 384 POPC molecules and 14592 water molecules (box size $\sim 10.75 \text{ nm} \times$

10.75 nm \times 8.04 nm). The CHARMM36 all-atom force field describes POPC molecules [65] and the TIP3P model is used for water molecules.[66] The van der Waals interactions are modeled using the Lennard-Jones potential with a cutoff radius of 1.2 nm. Electrostatic interactions are calculated with the particle mesh Ewald method, also employing a 1.2 nm cutoff.[67] Initially, the steepest descent algorithm is utilized to remove any unreasonable structures in the initial configuration.[68] The target temperature and pressure for all NPT simulations are set to 300 K and 1.01325 bar, respectively. Subsequently, a 100 ns simulation is conducted to ensure the system achieves equilibrium. The Bussi–Donadio–Parrinello thermostat [69] and the Berendsen semi-isotropic barostat are employed.[70] An additional 100 ns simulation is then performed for sampling, maintaining the temperature and pressure using the Nosé–Hoover thermostat [71, 72] and the Parrinello–Rahman semi-isotropic barostat, respectively.[73, 74] Throughout the simulations, the LINCS algorithm [75] is employed to constrain all bond lengths including hydrogen atoms, allowing for a larger integration time step, i.e., 2 fs.

Details of coarse-grained simulation

PACKMOL software [76] and CHARMM-GUI webserver[64] are utilized to construct the initial bilayer systems, each composing of 384 POPC molecules and 3649 water beads (box size \sim 11.02 nm \times 11.02 nm \times 7.67 nm). To consider the finite size effect on the optimized parameters, two systems of 21 nm \times 21 nm \times 17 nm and 31 \times 31 nm \times 27 nm are also investigated. The MARTINI2 force field [16] is employed in these simulations. Notably, 10% of the original water beads (P4 type) are replaced with anti-freezing water beads (BP4 type) to prevent freezing effects at lower temperatures and enhance system stability. The basic simulation settings are nearly identical to those used in the fine-grained simulations, with a few exceptions. A cutoff of 1.1 nm is chosen for nonbonded interactions to accelerate the simulations. The Bussi–Donadio–Parrinello thermostat [69] is selected for both equilibrium and production phases. The simulation time for equilibrium and production phases are 500 ns with a time step of 20.0 fs used throughout the simulations.

Analyses

The thickness and area per lipid (APL) are computed by LiPyphilic [77] using Freud,[78] and the volume per lipid (VPL) is calculated by OVITO.[79]

The lateral diffusion coefficient (D_L) of lipids in a bilayer is obtained via the Einstein relation:

$$D_L = \frac{1}{4} \lim_{t \rightarrow \infty} \frac{d}{dt} \left\langle \frac{1}{N} \sum_{i=1}^N |r_i(t_0 + \Delta t) - r_i(t_0)|^2 \right\rangle_{t_0}, \quad (13)$$

where N is the number of lipids, $r_i(t_0)$ is the position in the xy -plane of lipid i at a origin time t_0 , $r_i(t_0 + \Delta t)$ is the position at a lag time Δt , and the angular brackets denote an average over all origin times, t_0 . It is worth noting that the Martini dynamics are faster than all-atom dynamics due to smoother coarse-grained interactions and the absence of fine-grained friction. A standard conversion factor of 4 is used for interpreting simulation results, reflecting the speed-up in diffusion dynamics of Martini water compared to real water. Therefore, the diffusion coefficient value should be corrected by dividing them by 4.[16]

The isothermal area compressibility modulus (K_A) is computed from the fluctuation of the APL via

$$K_A = \frac{2k_B T \langle \text{APL} \rangle}{N \delta_{\text{APL}}^2}, \quad (14)$$

where k_B is Boltzmann constant, T is the temperature, $\langle \text{APL} \rangle$ is the average of APL, N is the total number of lipid and δ_{APL}^2 is the variance of APL.

MD settings and analysis of PEO Example

Details of fine-grained simulation

PACKMOL software [76] is utilized to construct the initial systems, each composing of 40 PEO molecules with a polymerization degree of 52 (box size $\sim 5.07 \text{ nm} \times 5.07 \text{ nm} \times 5.07 \text{ nm}$). The OPLS all-atom force field [80] is used to describe the PEO molecule, which is generated by the LigParGen web server [81] and employs CM1A-LBCC partial atomic charges.[82] The van der Waals interactions are modeled using the Lennard-Jones potential with a truncation radius of 1.2 nm, consistent with the POPC fine-grained simulation. Electrostatic interactions are handled using the Particle Mesh Ewald (PME) method, also with a cutoff of 1.2 nm.[67] Initially, the steepest descent algorithm is employed to remove any unreasonable structures in the initial configuration.[68] For all NPT simulations, the target pressure is set to 1.01325 bar. Following this, a 60 ns annealing process is conducted, where the temperature is gradually increased from 298 K to 1000 K and then reduced back to 298 K three times. Subsequently, a 140 ns simulation is performed to ensure the system achieves equilibrium. These two process use the Bussi–Donadio–Parrinello thermostat [69] and Berendsen barostat.[70] Finally, a 200 ns simulation is performed for sampling, with the system maintained at 298 K and 1.01325 bar using Nosé–Hoover thermostat [71, 72] and the Parrinello–Rahman semi-isotropic barostat,[73, 74] respectively. Throughout the simulations, the LINCS algorithm [75] is employed to constrain all bond lengths including hydrogen atoms, allowing for a larger integration time step, i.e., 2 fs.

Details of coarse-grained simulation

The system used for optimization consists of 40 PEO molecules (box size $\sim 5.11 \text{ nm} \times 5.11 \text{ nm} \times 5.11 \text{ nm}$). To consider the finite size effect on the optimized parameters, three larger systems with box lengths of 10 nm, 20 nm, and 30 nm are also investigated. The MARTINI3 force field [17] is employed in this section. We perform a 100 ns annealing process where the temperature is gradually increased from 298 K to 500 K and then decreased from 500 K to 298 K, repeating this process three times. A time step of 20 fs is applied in all simulations. Other simulation settings are kept the same as those used in the fine-grained simulation of PEO.

Analyses

NVT simulations on slabs (two-dimensional periodic) in simulation boxes with fixed size of $\sim 5.11 \text{ nm} \times 5.11 \text{ nm} \times 20 \text{ nm}$ are applied to calculate the surface tensions of polymer–vacuum interfaces. The surface tension is calculated using the diagonal elements of the

pressure tensor:

$$\gamma = \frac{L_z}{2} \left(\langle P_{zz} \rangle - \frac{\langle P_{xx} \rangle + \langle P_{yy} \rangle}{2} \right), \quad (15)$$

where $\langle P_{xx} \rangle$, $\langle P_{yy} \rangle$, and $\langle P_{zz} \rangle$ are the average diagonal elements of the pressure tensor.

The glass transition temperature (T_g) is calculated by monitoring the specific volume (reciprocal of the density) of the polymer as a function of temperature. The T_g is identified as the temperature at which there is a noticeable change in the slope of the specific volume-temperature curve (Fig. 5c and S4), indicating a transition from the glassy state to the rubbery state.

Data availability

The data that support the findings of this study are available from the authors upon reasonable request. The setup of the examples in this work can be accessed at <https://amofms.readthedocs.io/en/latest/example.html>

Code availability

AMOFMS is an open-source software package fully developed in Python3, using GRO-MACS [83, 84] and MDAnalysis [85] for molecular dynamics simulations and data extraction, respectively. The package is available for easy installation and upgrades through Anaconda Cloud and PiP, ensuring user-friendly accessibility. The source code is managed via GitHub (<https://github.com/Dropletsimuli/AMOFMS>), allowing users to download, customize, and contribute to the software’s development. Comprehensive documentation (<https://amofms.readthedocs.io>) is provided to facilitate usability.

Acknowledgments

This work was supported by the National Natural Science Foundation of China under Grant No. 22273112 and the National Key R&D Program of China (No. 2021YFB3803200).

References

- [1] Guo, X., Dong, X., Zou, G., Gao, H. & Zhai, W. Strong and tough fibrous hydrogels reinforced by multiscale hierarchical structures with multimechanisms. *Sci. Adv.* **9** (2023).
- [2] Chen, L., Nixon, R. & De Bo, G. Force-controlled release of small molecules with a rotaxane actuator. *Nature* **628**, 320–325 (2024).
- [3] Luke, J., Yang, E. J., Labanti, C., Park, S. Y. & Kim, J.-S. Key molecular perspectives for high stability in organic photovoltaics. *Nat. Rev. Mater.* **8**, 839–852 (2023).
- [4] Mao, J. *et al.* Molecular mechanisms and evolutionary robustness of a color switch in proteorhodopsins. *Sci. Adv.* **10** (2024).
- [5] Cayron, J., Oms, T., Schlechtweg, T., Zedek, S. & Van Melder, L. TisB protein is the single molecular determinant underlying multiple downstream effects of ofloxacin in *Escherichia coli*. *Sci. Adv.* **10** (2024).

- [6] Darby, E. M. *et al.* Molecular mechanisms of antibiotic resistance revisited. *Nat. Rev. Microbiol.* **21**, 280–295 (2023).
- [7] Noid, W. G. Perspective: Advances, Challenges, and Insight for Predictive Coarse-Grained Models. *J. Phys. Chem. B* **127**, 4174–4207 (2023).
- [8] Borges-Araújo, L. *et al.* Pragmatic Coarse-Graining of Proteins: Models and Applications. *J. Chem. Theory Comput.* **19**, 7112–7135 (2023).
- [9] van Teijlingen, A., Smith, M. C. & Tuttle, T. Short Peptide Self-Assembly in the Martini Coarse-Grain Force Field Family. *Acc. Chem. Res.* **56**, 644–654 (2023).
- [10] Coscia, B. J., Browning, A. R., Sanders, J. M. & Halls, M. D. Physics-based molecular modeling of biosurfactants. *Curr. Opin. Colloid Interface Sci.* **68**, 101760 (2023).
- [11] Parekh, P. Y., Patel, V. I., Khimani, M. R. & Bahadur, P. Self-assembly of bile salts and their mixed aggregates as building blocks for smart aggregates. *Adv. Colloid Interface Sci.* **312**, 102846 (2023).
- [12] Shi, R., Qian, H. & Lu, Z. Coarse-grained molecular dynamics simulation of polymers: Structures and dynamics. *WIREs Comput. Mol. Sci.* **13** (2023).
- [13] Zhu, Z., Luo, X. & Paddison, S. J. Coarse-Grained Modeling of Ion-Containing Polymers. *Chem. Rev.* **122**, 10710–10745 (2022).
- [14] Ingólfsson, H. I. *et al.* The power of coarse graining in biomolecular simulations. *WIREs Comput. Mol. Sci.* **4**, 225–248 (2014).
- [15] Jin, J., Pak, A. J., Durumeric, A. E. P., Loose, T. D. & Voth, G. A. Bottom-up Coarse-Graining: Principles and Perspectives. *J. Chem. Theory Comput.* **18**, 5759–5791 (2022).
- [16] Marrink, S. J., Risselada, H. J., Yefimov, S., Tieleman, D. P. & de Vries, A. H. The MARTINI Force Field: Coarse Grained Model for Biomolecular Simulations. *J. Phys. Chem. B* **111**, 7812–7824 (2007).
- [17] Souza, P. C. T. *et al.* Martini 3: a general purpose force field for coarse-grained molecular dynamics. *Nat. Methods* **18**, 382–388 (2021).
- [18] Alessandri, R. *et al.* Pitfalls of the Martini Model. *J. Chem. Theory Comput.* **15**, 5448–5460 (2019).
- [19] Majumder, A. & Straub, J. E. Addressing the Excessive Aggregation of Membrane Proteins in the MARTINI Model. *J. Chem. Theory Comput.* **17**, 2513–2521 (2021).
- [20] Jarin, Z., Newhouse, J. & Voth, G. A. Coarse-Grained Force Fields from the Perspective of Statistical Mechanics: Better Understanding of the Origins of a MARTINI Hangover. *J. Chem. Theory Comput.* **17**, 1170–1180 (2021).
- [21] Izvekov, S. & Voth, G. A. A Multiscale Coarse-Graining Method for Biomolecular Systems. *J. Phys. Chem. B* **109**, 2469–2473 (2005).
- [22] Izvekov, S. & Voth, G. A. Multiscale coarse graining of liquid-state systems. *J. Chem. Phys.* **123** (2005).
- [23] Izvekov, S. & Voth, G. A. Multiscale Coarse-Graining of Mixed Phospholipid/Cholesterol Bilayers. *J. Chem. Theory Comput.* **2**, 637–648 (2006).
- [24] Friederich, P., Häse, F., Proppe, J. & Aspuru-Guzik, A. Machine-learned potentials for next-generation matter simulations. *Nat. Mater.* **20**, 750–761 (2021).
- [25] Wang, J. *et al.* Machine Learning of Coarse-Grained Molecular Dynamics Force Fields. *ACS Cent. Sci.* **5**, 755–767 (2019).
- [26] Majewski, M. *et al.* Machine learning coarse-grained potentials of protein thermodynamics. *Nat. Commun.* **14**, 5739 (2023).

- [27] Dunn, N. J. H., Foley, T. T. & Noid, W. G. Van der Waals Perspective on Coarse-Graining: Progress toward Solving Representability and Transferability Problems. *Acc. Chem. Res.* **49**, 2832–2840 (2016).
- [28] Mancardi, G. *et al.* A computational view on nanomaterial intrinsic and extrinsic features for nanosafety and sustainability. *Mater. Today* **67**, 344–370 (2023).
- [29] Rühle, V., Junghans, C., Lukyanov, A., Kremer, K. & Andrienko, D. Versatile Object-Oriented Toolkit for Coarse-Graining Applications. *J. Chem. Theory Comput.* **5**, 3211–3223 (2009).
- [30] Mirzoev, A. & Lyubartsev, A. P. MagiC: Software Package for Multiscale Modeling. *J. Chem. Theory Comput.* **9**, 1512–1520 (2013).
- [31] McDonagh, J. L., Shkurti, A., Bray, D. J., Anderson, R. L. & Pyzer-Knapp, E. O. Utilizing Machine Learning for Efficient Parameterization of Coarse Grained Molecular Force Fields. *J. Chem. Inf. Model.* **59**, 4278–4288 (2019).
- [32] Empereur-Mot, C. *et al.* Swarm-CG : Automatic Parametrization of Bonded Terms in MARTINI-Based Coarse-Grained Models of Simple to Complex Molecules via Fuzzy Self-Tuning Particle Swarm Optimization. *ACS Omega* **5**, 32823–32843 (2020).
- [33] Empereur-mot, C. *et al.* Automatic multi-objective optimization of coarse-grained lipid force fields using SwarmCG. *J. Chem. Phys.* **156** (2022).
- [34] Mahajan, S. & Tang, T. Automated Parameterization of Coarse-Grained Polyethylenimine under a Martini Framework. *J. Chem. Inf. Model.* **63**, 4328–4341 (2023).
- [35] Peng, Y. *et al.* OpenMSCG: A Software Tool for Bottom-Up Coarse-Graining. *J. Phys. Chem. B* **127**, 8537–8550 (2023).
- [36] Stroh, K. S., Souza, P. C. T., Monticelli, L. & Risselada, H. J. CGCompiler: Automated Coarse-Grained Molecule Parametrization via Noise-Resistant Mixed-Variable Optimization. *J. Chem. Theory Comput.* **19**, 8384–8400 (2023).
- [37] Seo, S. & Shinoda, W. SPICA Force Field for Lipid Membranes: Domain Formation Induced by Cholesterol. *J. Chem. Theory Comput.* **15**, 762–774 (2019).
- [38] Marrink, S. J. & Tieleman, D. P. Perspective on the Martini model. *Chem. Soc. Rev.* **42**, 6801 (2013).
- [39] Li, Z. *et al.* Graph neural network based coarse-grained mapping prediction. *Chem. Sci.* **11**, 9524–9531 (2020).
- [40] Gilmer, J., Schoenholz, S. S., Riley, P. F., Vinyals, O. & Dahl, G. E. *Neural Message Passing for Quantum Chemistry*. *Proc. 34th Int. Conf. Mach. Learn.*, 1263–1272 (PMLR, 2017).
- [41] Xuan Vinh, N., Epps, J. & Bailey, J. Information Theoretic Measures for Clusterings Comparison: Variants, Properties, Normalization and Correction for Chance. *J. Mach. Learn. Res.* **11**, 2837–2854 (2010).
- [42] Campello, R. J. G. B., Moulavi, D. & Sander, J. *Density-based clustering based on hierarchical density estimates*. (eds Pei, J., Tseng, V. S., Cao, L., Motoda, H. & Xu, G.) *Adv. Knowl. Discov. Data Min.*, 160–172 (Springer Berlin Heidelberg, Berlin, Heidelberg, 2013).
- [43] Sarfraz, S., Sharma, V. & Stiefelhagen, R. *Efficient Parameter-Free Clustering Using First Neighbor Relations*. *2019 IEEE/CVF Conf. Comput. Vis. Pattern Recognit.*, 8926–8935 (IEEE, 2019).

- [44] Sarfraz, M. S., Koulakis, M., Seibold, C. & Stiefelhagen, R. *Hierarchical Nearest Neighbor Graph Embedding for Efficient Dimensionality Reduction*. 2022 IEEE/CVF Conf. Comput. Vis. Pattern Recognit., 336–345 (IEEE, 2022).
- [45] Dhillon, I. S., Guan, Y. & Kulis, B. Weighted Graph Cuts without Eigenvectors A Multilevel Approach. *IEEE Trans. Pattern Anal. Mach. Intell.* **29**, 1944–1957 (2007).
- [46] Karypis, G. & Kumar, V. A Fast and High Quality Multilevel Scheme for Partitioning Irregular Graphs. *SIAM J. Sci. Comput.* **20**, 359–392 (1998).
- [47] Ng, A., Jordan, M. & Weiss, Y. *On Spectral Clustering: Analysis and an algorithm*. *Adv. Neural Inf. Process. Syst.*, Vol. 14 (2001).
- [48] Mishra, A. *et al.* Multiobjective genetic training and uncertainty quantification of reactive force fields. *npj Comput. Mater.* **4**, 42 (2018).
- [49] Chan, H. *et al.* Machine learning coarse grained models for water. *Nat. Commun.* **10**, 379 (2019).
- [50] Weiel, M. *et al.* Dynamic particle swarm optimization of biomolecular simulation parameters with flexible objective functions. *Nat. Mach. Intell.* **3**, 727–734 (2021).
- [51] Kučerka, N., Tristram-Nagle, S. & Nagle, J. F. Structure of Fully Hydrated Fluid Phase Lipid Bilayers with Monounsaturated Chains. *J. Membr. Biol.* **208**, 193–202 (2006).
- [52] Smaby, J., Momsen, M., Brockman, H. & Brown, R. Phosphatidylcholine acyl unsaturation modulates the decrease in interfacial elasticity induced by cholesterol. *Biophys. J.* **73**, 1492–1505 (1997).
- [53] Pabst, G., Rappolt, M., Amenitsch, H. & Lagner, P. Structural information from multilamellar liposomes at full hydration: Full q -range fitting with high quality x-ray data. *Phys. Rev. E* **62**, 4000–4009 (2000).
- [54] Filippov, A., Orädd, G. & Lindblom, G. Influence of Cholesterol and Water Content on Phospholipid Lateral Diffusion in Bilayers. *Langmuir* **19**, 6397–6400 (2003).
- [55] Binder, H. & Gawrisch, K. Effect of Unsaturated Lipid Chains on Dimensions, Molecular Order and Hydration of Membranes. *J. Phys. Chem. B* **105**, 12378–12390 (2001).
- [56] Grünewald, F. *et al.* Polyply; a python suite for facilitating simulations of macromolecules and nanomaterials. *Nat. Commun.* **13**, 68 (2022).
- [57] Wixwat, W., Fu, Y. & Stevens, J. Index of refraction, density and viscosity measurements of poly(propylene glycol)-salt complexes. *Polymer* **32**, 1181–1185 (1991).
- [58] Singla, S. & Beckham, H. W. Miscible Blends of Cyclic Poly(oxyethylene) in Linear Polystyrene. *Macromolecules* **41**, 9784–9792 (2008).
- [59] Wang, X. *et al.* DMFF: An Open-Source Automatic Differentiable Platform for Molecular Force Field Development and Molecular Dynamics Simulation. *J. Chem. Theory Comput.* **19**, 5897–5909 (2023).
- [60] Gasteiger, J. & Marsili, M. Iterative partial equalization of orbital electronegativity—a rapid access to atomic charges. *Tetrahedron* **36**, 3219–3228 (1980).
- [61] Paszke, A. *et al.* *Pytorch: An imperative style, high-performance deep learning library*. *Adv. Neural Inf. Process. Syst.*, Vol. 32 (2019).
- [62] Fey, M. & Lenssen, J. E. *Fast graph representation learning with PyTorch Geometric*. *ICLR Workshop on Representation Learning on Graphs and Manifolds* (2019).
- [63] Lindahl, Abraham, Hess & van der Spoel. GROMACS 2021.4 Source code (2021).
- [64] Jo, S., Kim, T., Iyer, V. G. & Im, W. CHARMM-GUI: A web-based graphical user

- interface for CHARMM. *J. Comput. Chem.* **29**, 1859–1865 (2008).
- [65] Klauda, J. B. *et al.* Update of the CHARMM All-Atom Additive Force Field for Lipids: Validation on Six Lipid Types. *J. Phys. Chem. B* **114**, 7830–7843 (2010).
 - [66] Jorgensen, W. L., Chandrasekhar, J., Madura, J. D., Impey, R. W. & Klein, M. L. Comparison of simple potential functions for simulating liquid water. *J. Chem. Phys.* **79**, 926–935 (1983).
 - [67] Essmann, U. *et al.* A smooth particle mesh Ewald method. *J. Chem. Phys.* **103**, 8577–8593 (1995).
 - [68] Wardi, Y. A stochastic steepest-descent algorithm. *J. Optim. Theory Appl.* **59**, 307–323 (1988).
 - [69] Bussi, G., Donadio, D. & Parrinello, M. Canonical sampling through velocity rescaling. *J. Chem. Phys.* **126**, 014101 (2007).
 - [70] Berendsen, H. J. C., Postma, J. P. M., van Gunsteren, W. F., DiNola, A. & Haak, J. R. Molecular dynamics with coupling to an external bath. *J. Chem. Phys.* **81**, 3684–3690 (1984).
 - [71] Nosé, S. A molecular dynamics method for simulations in the canonical ensemble. *Mol. Phys.* **52**, 255–268 (1984).
 - [72] Hoover, W. G. Canonical dynamics: Equilibrium phase-space distributions. *Phys. Rev. A* **31**, 1695–1697 (1985).
 - [73] Parrinello, M. & Rahman, A. Polymorphic transitions in single crystals: A new molecular dynamics method. *J. Appl. Phys.* **52**, 7182–7190 (1981).
 - [74] Nosé, S. & Klein, M. Constant pressure molecular dynamics for molecular systems. *Mol. Phys.* **50**, 1055–1076 (1983).
 - [75] Hess, B., Bekker, H., Berendsen, H. J. C. & Fraaije, J. G. E. M. LINCS: A linear constraint solver for molecular simulations. *J. Comput. Chem.* **18**, 1463–1472 (1997).
 - [76] Martínez, L., Andrade, R., Birgin, E. G. & Martínez, J. M. PACKMOL: A package for building initial configurations for molecular dynamics simulations. *J. Comput. Chem.* **30**, 2157–2164 (2009).
 - [77] Smith, P. & Lorenz, C. D. LiPyphilic: A Python Toolkit for the Analysis of Lipid Membrane Simulations. *J. Chem. Theory Comput.* **17**, 5907–5919 (2021).
 - [78] Ramasubramani, V. *et al.* Freud: A software suite for high throughput analysis of particle simulation data. *Comput. Phys. Commun.* **254** (2020).
 - [79] Stukowski, A. Visualization and analysis of atomistic simulation data with OVITO—the Open Visualization Tool. *Model. Simul. Mater. Sci. Eng.* **18**, 015012 (2010).
 - [80] Jorgensen, W. L., Maxwell, D. S. & Tirado-Rives, J. Development and Testing of the OPLS All-Atom Force Field on Conformational Energetics and Properties of Organic Liquids. *J. Am. Chem. Soc.* **118**, 11225–11236 (1996).
 - [81] Dodda, L. S., Cabeza de Vaca, I., Tirado-Rives, J. & Jorgensen, W. L. LigParGen web server: an automatic OPLS-AA parameter generator for organic ligands. *Nucleic Acids Res.* **45**, W331–W336 (2017).
 - [82] Dodda, L. S., Vilseck, J. Z., Tirado-Rives, J. & Jorgensen, W. L. 1.14*CM1A-LBCC: Localized Bond-Charge Corrected CM1A Charges for Condensed-Phase Simulations. *J. Phys. Chem. B* **121**, 3864–3870 (2017).
 - [83] Van Der Spoel, D. *et al.* GROMACS: Fast, flexible, and free. *J. Comput. Chem.* **26**, 1701–1718 (2005).

- [84] Abraham, M. J. *et al.* GROMACS: High performance molecular simulations through multi-level parallelism from laptops to supercomputers. *SoftwareX* **1-2**, 19–25 (2015).
- [85] Michaud-Agrawal, N., Denning, E. J., Woolf, T. B. & Beckstein, O. MDAAnalysis: A toolkit for the analysis of molecular dynamics simulations. *J. Comput. Chem.* **32**, 2319–2327 (2011).